Finite-size effects on the phase structure of the Walecka model

L. M. Abreu* and E. S. Nery†
Instituto de Física, Universidade Federal da Bahia, Salvador, Bahia 40210-340, Brazil
(Received 24 July 2017; published 15 November 2017)

In this work we investigate the finite-size effects on the phase structure of the Walecka model within the framework of a generalized ζ-function, focusing on the influence of temperature as well as the number and length of compactified spatial dimensions. Here we concentrate on the situation of larger values of the coupling between the scalar and fermion fields, in which a phase transition of first order takes place. The phase transitions are analyzed and compared with the system in the situations of one, two, and three compactified spatial dimensions. Our findings suggest that the thermodynamic behavior of the system depends on the length and number of spatial dimensions, with the symmetric phase being favored as the size of the system diminishes.

DOI: 10.1103/PhysRevC.96.055204

I. INTRODUCTION

One of the most interesting questions that has been receiving a great deal of attention in hadron and nuclear physics concerns the study of strongly interacting matter properties under the changes of the environment. As examples, we can highlight several phenomena: the phase diagram of nuclear and quark matter, relativistic degenerate gas phase transitions, quark-gluon plasma formation in heavy-ion collisions, the phase structure of neutron stars, and so on [1,2].

In light of the theoretical grounds to treat these physical systems, effective quantum field theories of quantum chromodynamics (QCD) at finite temperature have proved to be very useful tools. In particular, one emblematic example is the Walecka model [3]. Different versions of this model have been largely employed as a laboratory to get insights on the thermodynamic behavior of hadronic matter, describing a reasonable number of phenomena in the sector of strong interactions (for reviews, see Refs. [4–21]).

A representative system which has been understood at least qualitatively via Walecka-like models is that of nuclear matter, whose the exchange nucleon-nucleon interactions are discussed. Considering the scenario of finite-temperature field theory, it can be thought of as a gas of nucleons (associated with the Dirac field) embedded in a bath of scalar, vector, and other types of particles constituting the hot and dense hadronic medium (associated with scalars, vectors, and other fields). Therefore, interesting aspects of thermodynamic properties of this system can be investigated under certain conditions, such as finite temperature, finite chemical potential, external magnetic field, and others [2–21].

Besides, there is a vast bibliography on the subject of the of finite-size effects on the thermodynamics of effective field theories for different physical phenomena. Some interesting examples of these works are in Refs. [22–48]. The general question treated in these cited works is to estimate the relevance of the fluctuations owing to finite-size effects in the thermodynamic properties of the system. In particular, within the approach of a scalar version of the Yukawa model, it is argued in Refs. [41,42] that the reduction of the size of the reservoir which encloses the boson gas might favor the symmetrical phase.

Thus, taking as motivation the discussion done above, in this work we perform an investigation about the influence of the boundaries on the thermodynamic behavior of Walecka's mean-field theory without quantum correction. In the present study we make use of mean-field approximation for the real scalar and vector fields, which could be associated with a first-order estimate of the thermodynamic properties of hadron matter [4]. This engenders the interpretation of a thermal gas of fermions confined in a reservoir and interacting with a medium constituted of other hadrons. We treat jointly spatial compactification and the introduction of finite temperature, using a generalized Matsubara prescription [49] and a ζ-function regularization method [22,26,29,35,38,50,51]. The thermodynamic potential and gap equations can be determined analytically, and the phase structure is analyzed under the change of temperature, as well as the number and length of compactified spatial dimensions.

The paper is organized as follows. In Sec. II, we present the model and calculate the relevant thermodynamic quantities using the ζ-function regularization approach. In particular, in Secs. II A and II B we introduce the situation without and with boundaries, respectively. Section III is devoted to the discussion of the thermodynamics of this system. Finally, Sec. IV presents some concluding remarks.

II. THE MODEL

Let us introduce the effective Lagrangian density of the Walecka model. It describes a Dirac field interacting with scalar and vector fields, denoted, respectively, as ψ, σ, and ω, and is given by

$$\begin{aligned}\mathcal{L} = {} & \bar{\psi}(i\gamma^{\mu}\partial_{\mu} - m_{\psi} + g_{\sigma}\sigma - g_{\omega}\gamma^{\mu}\omega_{\mu})\psi \\ & + \tfrac{1}{2}\left(\partial_{\mu}\sigma\,\partial^{\mu}\sigma - m_{\sigma}^{2}\sigma^{2}\right) - \tfrac{1}{4}W^{\mu\nu}W_{\mu\nu} \\ & + \tfrac{1}{2}m_{\omega}^{2}\omega_{\mu}\omega^{\mu}, \end{aligned} \tag{1}$$

where m_{ψ}, m_{σ}, and m_{ω} are the masses of the Dirac, scalar, and vector fields, respectively; $W_{\mu\nu} = \partial_{\mu}\omega_{\nu} - \partial_{\nu}\omega_{\mu}$ is the

*luciano.abreu@ufba.br
†elenilsonnery@hotmail.com

 ©2017 American Physical Society

ω-field strength tensor; and g_σ (g_ω) is the coupling constant for interaction between the Dirac and scalar (vector) field.

In the Lorentz gauge, $\partial_\mu \omega^\mu = 0$, the equations of motion obtained from Eq. (1) are

$$[\gamma^\mu(\partial_\mu - i g_\omega \omega_\mu) + m_\psi - g_\sigma \sigma]\psi = 0, \tag{2}$$

$$\left(\partial_\mu \partial^\mu + m_\sigma^2\right)\sigma = g_\sigma \rho_s, \tag{3}$$

$$\left(\partial_\mu \partial^\mu + m_\omega^2\right)\omega_\nu = i g_\omega j_\nu, \tag{4}$$

where $\rho_s = \bar{\psi}\psi$ is the scalar density and $j^\mu = \bar{\psi}\gamma^\mu\psi$ the fermion 4-current. Therefore, we have a system of three coupled equations to solve.

The lowest-order estimate of the thermodynamic properties of the ψ field interacting with other fields can be performed by considering the mean-field approximation. It means that we will neglect the fluctuations of the scalar and vector fields. In this sense, the σ and ω fields are replaced with their classical counterparts, i.e.,

$$\begin{aligned} \sigma &= \langle\sigma\rangle, \\ \omega &= \langle\omega^0\rangle, \end{aligned} \tag{5}$$

with $\omega^\mu = 0$ for $\mu \neq 0$. Then, in mean-field approximation the Lagrangian density in Eq. (1) can be rewritten as

$$\begin{aligned} \bar{\mathcal{L}} = \bar{\psi}[i\gamma^\mu\partial_\mu - (m_\psi - g_\sigma\langle\sigma\rangle) - g_\omega\gamma^0\langle\omega_0\rangle]\psi \\ -\tfrac{1}{2}m_\sigma^2\langle\sigma\rangle^2 + \tfrac{1}{2}m_\omega^2\langle\omega^0\rangle^2, \end{aligned} \tag{6}$$

and the equations of motion in Eqs. (3) and (4) become

$$[\gamma^\mu\partial_\mu + (m_\psi - g_\sigma\langle\sigma\rangle)]\psi = g_\omega\gamma_0\langle\omega^0\rangle\psi, \tag{7}$$

$$\langle\sigma\rangle = \left(\frac{g_\sigma}{m_\sigma^2}\right)\rho_s, \tag{8}$$

$$\langle\omega_0\rangle = \left(\frac{g_\omega}{m_\omega^2}\right)\rho, \tag{9}$$

where $\rho = j^0 = \bar{\psi}\gamma^0\psi$ is the fermion density.

To investigate the thermodynamic properties of the model introduced above within imaginary time formalism [2,49], we assume that the system is in equilibrium at a temperature T and chemical potential (density) μ. So, we define the grand partition function in a D-dimensional Euclidean spacetime at finite temperature T and d compactified spatial dimensions,

$$\begin{aligned} \mathcal{Z} = \int \mathcal{D}\psi^\dagger\mathcal{D}\psi \\ \times \exp\left\{-\int_0^\beta d\tau \prod_{i=1}^{d}\int_0^{L_i} dx_i \int d^{D-\delta}\vec{z}[\bar{\mathcal{L}}_E + \mu j_0]\right\}, \end{aligned} \tag{10}$$

where $\beta = 1/T$; $\delta = d + 1 \leqslant D$; $\{L_i\}$ are the compactification lengths of the spatial coordinates; $\bar{\mathcal{L}}_E$ is the Lagrangian density given by Eq. (6) in Euclidean space; and μ is the fermion (baryonic) chemical potential. Finite-size and temperature effects are taken into account along the prescription described in Ref. [50]: Each spatial coordinate x_i is compactified in a length L_i and, as usual, imaginary time is compactified in the range $[0,\beta]$. A vector in the D-dimensional spacetime is given by $\mathbf{u} = (\tau, x_1, x_2, \ldots, x_d, \vec{z})$, where τ is the imaginary time, $(x_1, x_2, \ldots, x_d)$ correspond to the compactified spatial coordinates, and $\vec{z}$ is a $(D-\delta)$-dimensional vector. The Fourier dual of $\mathbf{u}$ is a D-dimensional vector in momentum space, $\mathbf{q} = (k_\tau, k_{x_1}, \ldots, k_{x_d}, \vec{p})$, with $\vec{p}$ being the corresponding momentum to $\vec{z}$. As a consequence, in explicit calculations temperature and finite-size effects are implemented through the following modifications in the Feynman rules,

$$\begin{aligned} \int \frac{d^D q}{(2\pi)^D} f(q) \to \frac{1}{\beta L_i \times \cdots \times L_d} \\ \times \sum_{l,\{n_i\}=-\infty}^{\infty} \int \frac{d^{D-\delta}p}{(2\pi)^{D-\delta}} f(\omega_l, \{\omega_{n_i}\}, p), \end{aligned} \tag{11}$$

where $\{n_i\} \equiv n_1, \ldots, n_d$; $\{\omega_i\} \equiv \omega_1, \ldots, \omega_d$; in the right-hand side, we have performed the replacements

$$k_\tau \to \omega_l = \frac{2\pi}{\beta}\left(l + \frac{1}{2}\right) - i\mu, \quad l = 0, \pm 1, \pm 2, \ldots,$$

$$k_{x_i} \to \omega_{n_i} = \frac{2\pi}{L}(n_i + c), \qquad n_i = 0, \pm 1, \pm 2, \ldots,$$

with $c = 0$ or $c = 1/2$ for periodic or antiperiodic spatial boundary conditions, respectively. In the present study we use the antiperiodic spatial boundary conditions.

Then, after the integration of the fields $\psi^\dagger$ and ψ, we can obtain from Eq. (10) the thermodynamic potential,

$$\begin{aligned} U(T, \{L_i\}, \mu_{\text{eff}}) &\equiv \frac{1}{\beta}\ln\mathcal{Z} \\ &= \frac{V}{2}\left[m_\sigma^2\langle\sigma\rangle^2 - m_\omega^2\langle\omega^0\rangle^2\right] \\ &\quad - \frac{\gamma V}{\beta L_i \times \cdots \times L_d} Y'(0), \end{aligned} \tag{12}$$

where γ is the degeneracy factor (we adopt here $\gamma = 4$ [4]), V is the volume, and $Y(s)$ is the multiple sum obtained after performing the integration over the $(D-\delta)$-dimensional momentum vector remaining from the prescription in Eq. (11),

$$\begin{aligned} Y(s) = J(s,\delta) \sum_{l,n_1,\ldots,n_d=-\infty}^{\infty} \left\{\left[\frac{2\pi}{\beta}\left(l + \frac{1}{2}\right) - i\mu_{\text{eff}}\right]^2 \right. \\ \left. + \sum_{i=1}^{d}\left[\frac{2\pi}{L_i}\left(n_i + \frac{1}{2}\right)\right]^2 + m_{\text{eff}}^2\right\}^{-s+\frac{D-\delta}{2}}, \end{aligned} \tag{13}$$

with

$$J(s,\delta) = \frac{1}{(4\pi)^{(D-\delta)/2}} \frac{\Gamma\left(s - \frac{D-\delta}{2}\right)}{\Gamma(s)}. \tag{14}$$

$Y'(s)$ in Eq. (13) represents the derivative of $Y(s)$ with respect to the argument s; m_{eff} and μ_{eff} are, respectively, the effective mass and chemical potential of the fermion field and are given by

$$m_{\text{eff}} = m_\psi - g_\sigma\langle\sigma\rangle, \tag{15}$$

$$\mu_{\text{eff}} = \mu - g_\omega\langle\omega^0\rangle. \tag{16}$$

Then, modifications of the scalar and vector mean fields [whose allowed values are obtained from the solutions of gap equations in Eqs. (8) and (9)] change the mass and chemical potential of the fermions. We can interpret this as follows: The mass and density of fermions (for instance nucleons) are effectively modified due to their interactions with the hot and dense medium in which they are immersed.

It is relevant to notice that the multiple sum in Eq. (13) is the well-known Epstein-Hurwitz inhomogeneous ζ function [51], whose analytical continuation valid in the whole complex ν plane has the representation

$$
\begin{aligned}
A_{\delta}^{C^2}(\nu,\{a_i\},\{b_i\}) &= \sum_{\{n_i\}=-\infty}^{\infty}\left[\sum_{i=1}^{\delta} a_i(n_i-b_i)^2 + C^2\right]^{-\nu} \\
&= \frac{\pi^{\delta/2}}{\sqrt{a_1\times\cdots\times a_\delta}\,\Gamma(\nu)}\left\{\Gamma\left(\nu-\frac{\delta}{2}\right)C^{\delta-2\nu} + 2\sum_{i=1}^{\delta}\sum_{n_i=1}^{\infty}\cos(2\pi n_i b_i)\left(\frac{\pi n_i}{\sqrt{a_i}C}\right)^{\nu-\frac{\delta}{2}} K_{\nu-\frac{\delta}{2}}\left(\frac{2\pi n_i C}{\sqrt{a_i}}\right)\right. \\
&\quad + 2^2\sum_{i<j=1}^{\delta}\sum_{n_i,n_j=1}^{\infty}\cos(2\pi n_i b_i)\cos(2\pi n_j b_j)\left(\frac{\pi}{C^2}\sqrt{\frac{n_i^2}{a_i}+\frac{n_j^2}{a_j}}\right)^{\nu-\frac{\delta}{2}} K_{\nu-\frac{\delta}{2}}\left(2\pi C\sqrt{\frac{n_i^2}{a_i}+\frac{n_j^2}{a_j}}\right) \\
&\quad \left. + \cdots + 2^{\delta}\sum_{n_1,\ldots,n_\delta=1}^{\infty}\prod_{i=1}^{\delta}[\cos(2\pi n_i b_i)]\left(\frac{\pi}{C^2}\sqrt{\sum_{i=1}^{\delta}\frac{n_i^2}{a_i}}\right)^{\nu-\frac{\delta}{2}} K_{\nu-\frac{\delta}{2}}\left(2\pi C\sqrt{\sum_{i=1}^{\delta}\frac{n_i^2}{a_i}}\right)\right\}, \qquad (17)
\end{aligned}
$$

where K_ν is the modified Bessel function of the second kind.

Thus, the grand thermodynamic potential can be obtained by taking the derivative of the function $Y(s)$ in Eq. (17) and placing the result into Eq. (12). In Eq. (12) we have $\nu = s - (D-\delta)/2$, which engenders the label of the Bessel functions equal to $\nu - \delta/2 = s - D/2$. Therefore, for $D = 4$ the Bessel functions are K_{s-2} independently of the value of δ.

In addition, to study the thermodynamic behavior of the system, we need to consider the state equations of mean fields $\langle\sigma\rangle$ and $\langle\omega^0\rangle$,

$$\frac{\partial U}{\partial\langle\sigma\rangle} = 0, \qquad (18)$$

$$\frac{\partial U}{\partial\langle\omega^0\rangle} = 0. \qquad (19)$$

The solutions of these equations give the values of $\langle\sigma\rangle$ and $\langle\omega^0\rangle$ corresponding to the extrema of the grand thermodynamic potential U, where the system reaches the the equilibrium configuration. In this sense, we are interested in the fermion effective mass $m_{\rm eff} = m_{\rm eff}(T,\mu_{\rm eff},\{L_i\})$ defined in Eq. (15), which will be a $(T,\mu_{\rm eff},\{L_i\})$-dependent order parameter which governs the phase diagram of the model.

A. System without spatial boundaries ($d = 0$)

For completeness, we begin with the usual case where the system is in the absence of boundaries. It means that we use the recurrence formula in Eq. (17), with $D = 4$ and $\delta = 1$, identifying $a_1 = (\frac{2\pi}{\beta})$ and $b_1 = -i\frac{\mu_{\rm eff}\beta}{2\pi} + \frac{1}{2}$, and after that we replace the expression obtained for $Y(s)$ in Eq. (13). Nevertheless, we must perform the pole structure analysis in the calculations of the derivative of $Y(s)$ with respect to s, where $s \to 0$, before using it in the expression of thermodynamic potential (12). Accordingly, it can be remarked that for any regular function $G(s)$, we have $\lim_{s\to0}(d/ds)[G(s)/\Gamma(s)] = G(0)$.

Then, after performing the derivative of $Y(s)$ given in Eq. (13) with respect to s for $\epsilon \to 0$, but with the observations mentioned above in mind, we can rewrite the thermodynamic potential as

$$
\begin{aligned}
\frac{U(T,\mu_{\rm eff})}{V} &= \frac{1}{2}m_\sigma^2\langle\sigma\rangle^2 - \frac{1}{2}m_\omega^2\langle\omega^0\rangle^2 - U_{\rm vac} + \frac{\gamma}{\pi^2}\sum_{l=1}^{\infty}(-1)^l \\
&\quad\times\cosh(\beta l\mu_{\rm eff})\left(\frac{m_{\rm eff}}{l\beta}\right)^2 K_2(l\beta m_{\rm eff}), \qquad (20)
\end{aligned}
$$

where $U_{\rm vac}$ is the vacuum fluctuation energy per unit volume, i.e., the quantum correction, associated with the first term in the second line of Eq. (17). This contribution can be better understood from the discussions available in Refs. [52–54]: Because the scalar interaction effectively changes the fermion mass from m_ψ to $m_{\rm eff} = m_\psi - g_\sigma\langle\sigma\rangle$, it induces an energy density shift of the vacuum of magnitude

$$
\begin{aligned}
U_{\rm vac} &\propto \left[\frac{1}{(4\pi)^{\frac{D}{2}-1}}\Gamma\left(-\frac{D}{2}\right)m_{\rm eff}^D\right]_{D=4} \\
&\quad -\left[\frac{1}{(4\pi)^{\frac{D}{2}-1}}\Gamma\left(-\frac{D}{2}\right)m_\psi^D\right]_{D=4}, \qquad (21)
\end{aligned}
$$

where the second term on the right-hand side of the equation above has been introduced to eliminate the physically meaningless constant shift of the energy. Clearly, this expression contains divergences, which can be canceled by a renormalization procedure, as done in Refs. [52,54]. However, it is relevant to notice that in the present work we are interested

in the finite-size effects on the phase structure of the model introduced in Ref. [4]. In other words, we investigate the influence of boundaries on the thermodynamic behavior of Walecka's mean-field theory, without quantum correction. Therefore, henceforth we will omit in the calculations the term in Eq. (21). In this sense, the present analysis can be considered as a starting point for further work in which the quantum corrections might be considered.

Thus, the relevant thermodynamic properties can be derived from the grand thermodynamic potential in Eq. (20). The substitution of Eq. (20) in Eqs. (18) and (19) allows us to rewrite the gap equations as

$$\langle\sigma\rangle = \frac{g_\sigma}{m_\sigma^2}\rho_s, \tag{22}$$

$$\langle\omega^0\rangle = -\frac{\omega}{m_\omega^2}\rho, \tag{23}$$

where ρ_s and ρ are the scalar and number densities, respectively, given by

$$\rho_s = \frac{m_{\rm eff}^2}{\pi^2\beta}\sum_{l=1}^{\infty} a_l \cosh(l\beta\mu_{\rm eff})K_1(l\beta m_{\rm eff}), \tag{24}$$

$$\rho = \frac{m_{\rm eff}^2}{\pi^2\beta}\sum_{l=1}^{\infty} b_l \sinh(l\beta\mu_{\rm eff})K_2(l\beta m_{\rm eff}), \tag{25}$$

with $a_l = \frac{(-1)^{l-1}}{l}$ and $b_l = -2\frac{(-1)^{l-1}}{l}$.

B. System with compactified spatial dimensions ($d = 1,2,3$)

Now we present the model under question with the presence of boundaries, in the scenarios of $d = 1$, 2, and 3 compactified spatial coordinates.

We start by considering the simplest case, which is just one spatial compactification, $d = 1$, corresponding to a reservoir in the form of an infinite hollow slab of thickness $L_1 \equiv L$, in with the system at equilibrium and at a temperature β^{-1}. Then, to obtain the thermodynamic potential, we use Eqs. (13) and (17), with $D = 4$ and $\delta = 2$, and introduce the notation $a_1 = (\frac{2\pi}{\beta})$, $a_2 = (\frac{2\pi}{L})$, $b_1 = -i\frac{\mu_{\rm eff}\beta}{2\pi} + \frac{1}{2}$, and $b_2 = \frac{1}{2}$. Then, proceeding similarly as the way to find Eqs. (20), (22), and (23), the grand thermodynamic potential in Eq. (20) becomes

$$\begin{aligned}\frac{U(T,\mu_{\rm eff},L)}{V} &= \frac{1}{2}m_\sigma^2\langle\sigma\rangle^2 - \frac{1}{2}m_\omega^2\langle\omega^0\rangle^2 + U_{\rm vac} \\ &+ \sum_{l=1}^{\infty}(-1)^l\cosh(l\,\beta\,\mu_{\rm eff})\left(\frac{m_{\rm eff}}{l\,\beta}\right)^2 K_2(l\,m_{\rm eff}\,\beta) + \sum_{n=1}^{\infty}(-1)^n\left(\frac{m_{\rm eff}}{n\,L}\right)^2 K_2(n\,m_{\rm eff}\,L) \\ &+ \sum_{l,n=1}^{\infty}(-1)^{l+n-1}\cosh(l\beta\mu_{\rm eff})\left(\frac{m_{\rm eff}}{\sqrt{\beta^2l^2+L^2n^2}}\right)^2 K_2\left(m_{\rm eff}\sqrt{\beta^2l^2+L^2n^2}\right).\end{aligned} \tag{26}$$

Then, the use of Eq. (26) in the gap equations (18) and (19) and after some mathematical manipulations yield gap equations similar to those shown in Eqs. (22) and (23), but with the scalar and number densities in the present case, with $d = 1$ being respectively given by

$$\rho_s = A\left[\sum_{i=0}^{1}\sum_{n_i=1}^{\infty}\frac{d_{n_i}}{L_i}\cosh(\delta_{0i}n_iL_i\mu_{\rm eff})K_1(n_im_{\rm eff}L_i) + 2\sum_{n,l=1}^{\infty}c_{n,l}\cosh(l\beta\mu_{\rm eff})K_1\left(m_{\rm eff}\sqrt{\sum_{i=0}^{1}L_i^2n_i^2}\right)\right], \tag{27}$$

$$\rho = -4\pi^2A^2\left[\sum_{l=1}^{\infty}\frac{b_l}{2\beta}\,\mathrm{senh}(l\beta\mu_{\rm eff})K_2(lm_{\rm eff}\beta) - 2\beta\sum_{l,n=1}^{\infty}b_{l,n}\,\mathrm{senh}(n\beta\mu_{\rm eff})K_2\left(m_{\rm eff}\sqrt{\sum_{i=0}^{1}L_i^2n_i^2}\right)\right], \tag{28}$$

where $A = \frac{m_{\rm eff}}{\pi^2}$, $d_{n_0} = a_l$, $d_{n_1} = c_n$, $c_{n,l} = \frac{(-1)^{n+l}}{\sqrt{\sum_{i=0}^{1}L_i^2n_i^2}}$, and $b_{n,l} = \frac{2(-1)^{n+l}}{\sqrt{\sum_{i=0}^{1}L_i^2n_i^2}}$; also, we use the notation $L_0 \equiv \beta$, $L_1 \equiv L$, and $n_0 \equiv l$ and $n_1 \equiv n$.

We also analyze the present approach with two compactified spatial coordinates ($d = 2$), in which the reservoir has the geometry of a hollow, infinitely long wire with a rectangular cross section. In this context we return to Eqs. (13) and (17), with $D = 4$ and $\delta = 3$, and introduce the quantities $a_1 = (\frac{2\pi}{\beta})$, $a_2 = (\frac{2\pi}{L_1})$, $a_3 = (\frac{2\pi}{L_2})$, $b_1 = -i\frac{\mu_{\rm eff}\beta}{2\pi} + \frac{1}{2}$, $b_2 = \frac{1}{2}$, and $b_3 = \frac{1}{2}$. Then, proceeding in a way to similar to that found Eqs. (20), (22), and (23), the (L_1,L_2)-dependent expressions for grand thermodynamic potential in Eq. (20), gap equations in Eqs. (18) and (19), and number and scalar densities can be generated after some manipulations. For brevity, we omit these expressions because the reader can obtain them for himself.

Finally, looking at the case of three compactified spatial coordinates ($d = 3$), the reservoir has the form of parallelepipedal box of volume $L_1 \times L_2 \times L_3$. Once more, $Y(s)$ can be be obtained by taking $D = 4$ and $\delta = 4$ in Eqs. (13) and (17) and introducing the quantities $a_1 = (\frac{2\pi}{\beta})$, $a_2 = (\frac{2\pi}{L_1})$, $a_3 = (\frac{2\pi}{L_2})$, $a_3 = (\frac{2\pi}{L_3})$, $b_1 = -i\frac{\mu_{\rm eff}\beta}{2\pi} + \frac{1}{2}$, $b_2 = \frac{1}{2}$, $b_3 = \frac{1}{2}$, and $b_4 = \frac{1}{2}$. Hence, (L_1,L_2,L_3)-dependent expressions for the thermodynamic potential, scalar and number densities, pressure, entropy, and other thermodynamic quantities are determined by procedures similar to those described above.

In next section we will carry out the discussion of the thermodynamics of the model in these different situations.

III. PHASE STRUCTURE AND COMMENTS

Now we are able to analyze the thermodynamic behavior of the system previously introduced.

In the present approach, we consider the case in which the system is at effective chemical equilibrium, i.e., $\mu_{\rm eff} = 0$. It can be seen from Eqs. (24) and (25) that this constraint engenders $\rho = 0$ and therefore yields vanishing solutions for the $\langle\omega^0\rangle$ field in all cases of compactified spatial dimensions. It means that in the present analysis the numbers of fermion particles and antiparticles are equal. Therefore, we focus on the thermodynamics of the system as a function of the solutions of the gap equation (24) for $\langle\sigma\rangle = \langle\sigma\rangle(T, L_i)$ or $m_{\rm eff} = m_{\rm eff}(T, L_i)$ at $\langle\omega^0\rangle = 0$.

For convenience, all physical quantities are scaled by units of mass of the fermion field ψ, m_ψ:

$$\frac{U}{m_\psi^4} \to U, \quad \frac{T}{m_\psi} \to T, \quad \frac{\mu}{m_\psi} \to \mu, \quad \frac{\sigma}{m_\psi} \to \sigma, \\ \frac{m_\sigma}{m_\psi} \to m_\sigma, \quad \frac{m_{\rm eff}}{m_\psi} \to m_{\rm eff}, \quad L m_\psi \to L. \tag{29}$$

The discussion about the phase structure of the present model is accomplished under changes of the relevant parameters, paying attention to the influence of the number of compactified spatial dimensions. In this sense, the phase transitions are analyzed and compared with the system in the situations of one, two, and three compactified spatial dimensions. To make this comparison more accessible, the length of all spatial compactified coordinates is set to be the same, i.e., $L_i \equiv L$. This choice reduces the system to the following scenarios for $d = 1$, 2, and 3: confined between two parallel planes a distance L apart; confined to an infinitely long cylinder having a square transversal section of area L^2; and to a cubic box of volume L^3.

A. System without spatial boundaries ($d = 0$)

For completeness, we begin with a qualitative analysis of the behavior of the effective mass $m_{\rm eff}$ under changes of the relevant parameters but without the presence of boundaries, similarly to the scenario described in Ref. [4].[1] In what follows, including the figures, all parameters are understood to be redefined by the scaling in Eq. (29).

In Figs. 1 and 2 are plotted the values of $m_{\rm eff}$ that are solutions of the gap equation in Eq. (22) as function of temperature, by taking arbitrary values of the coupling constant g_σ. As discussed in Ref. [4], the increasing of the magnitude of the interaction between the σ and the ψ fields makes the system undergo a phase transition at a smaller critical temperature. This can be understood from the role of the σ field in binding the fermion particles: The increasing of the magnitude of attractive interaction between the fermions makes them more strongly bound, reducing the effective mass. Furthermore, the nature of the phase transition depends strongly on the strength of the coupling constant g_σ. For the case with lowest g_σ the dependence of $m_{\rm eff}$ on T is continuous, while for larger g_σ

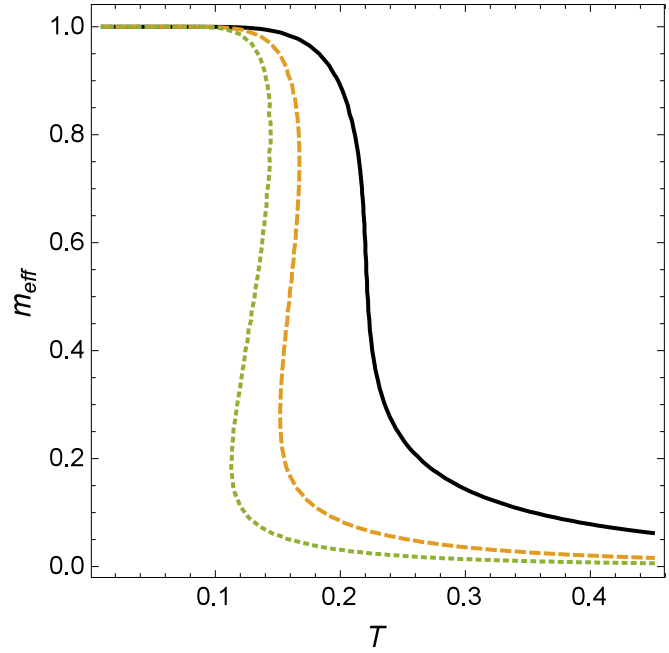

FIG. 1. Plot of values of $m_{\rm eff}$ that are solutions of the gap equation in Eq. (22) for $d = 0$ as a function of temperature at chemical equilibrium. We fix $m_\sigma = 0.53$. Solid, dashed, and dotted lines represent, respectively, the cases for $g_\sigma = 8.00$, $g_\sigma = 16.00$, and $g_\sigma = 26.00$.

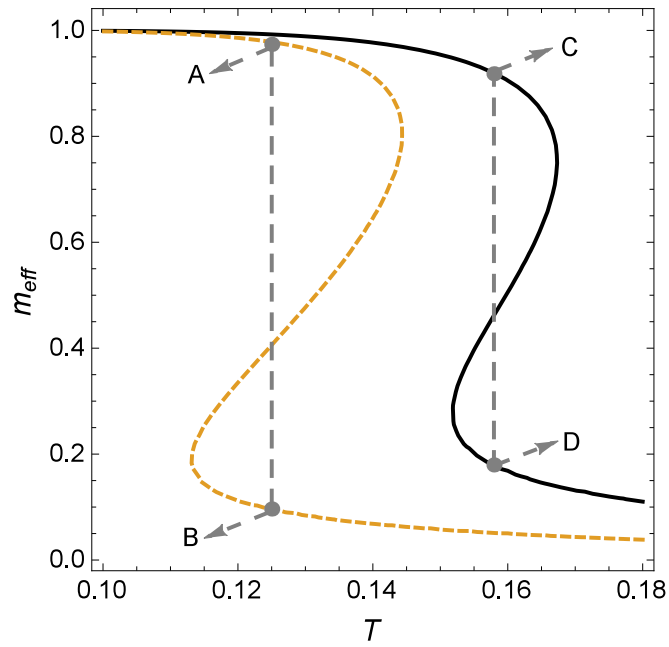

FIG. 2. Same as in Fig. 1, but with solid and dashed lines representing, respectively, the cases for $g_\sigma = 16.00$ and $g_\sigma = 26.00$, and with the temperature axis in the range near the transition point.

[1] We notice that we use a different scaling and notation with respect to Ref. [4].

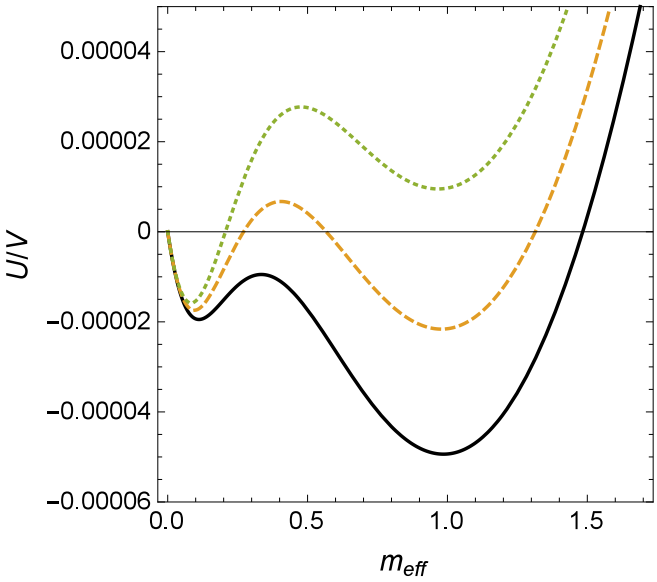

FIG. 3. Plot of normalized thermodynamic potential density in Eq. (30) for $d = 0$ as a function of effective mass and at chemical equilibrium. We fix $m_\sigma = 0.53$ and $g_\sigma = 26.00$. Solid, dashed, and dotted lines represent the cases for $T = 0.120$, $T = 0.125$, and $T = 0.130$, respectively.

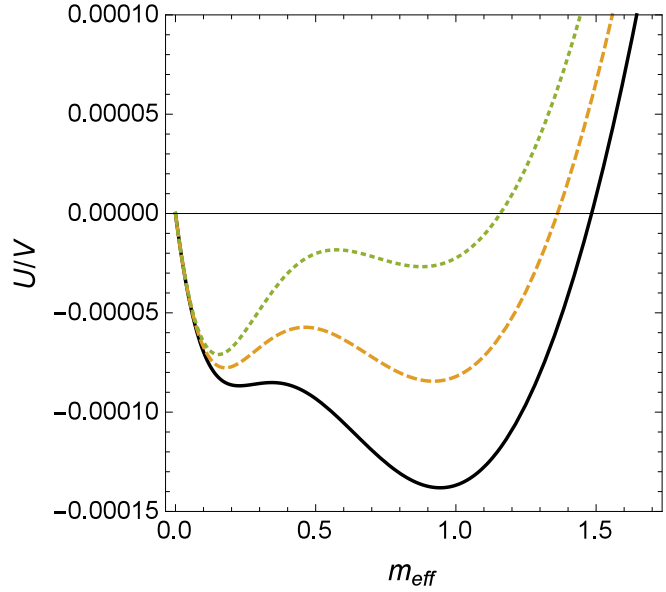

FIG. 4. Same as in Fig. 3, but with $g_\sigma = 16.00$. Solid, dashed, and dotted lines represent the cases for $T = 0.153$, $T = 0.158$, and $T = 0.163$, respectively.

the curves cross twice, characterizing a discontinuous phase transition.

Specifically, in Fig. 2 are plotted the solutions for $m_{\rm eff}$ as a function of temperature for larger values of g_σ, which engender a first-order transition, with the temperature axis in the range near the transition point. The points $\overline{AB}$ and $\overline{CD}$ indicate the ordered pairs of coordinates $(m_{\rm eff}, T)$ of the intersections that give the values of the critical temperature and $m_{\rm eff}$ at both end points of the mixed phase. In the case of $g_\sigma = 26.00$ the jump occurs at $T \approx 0.125$–0.126, where the effective mass changes from ≈ 0.98 to ≈ 0.1, while for $g_\sigma = 16.00$ the phase transition is at $T \approx 0.158$–0.159, where $m_{\rm eff}$ goes from ≈ 0.90 to ≈ 0.20. At high temperatures, the system behaves like an almost-free zero-mass fermion gas.

It is worth mentioning that a more detailed study of the scenario above for several values of g_σ gives the following result: For $g_\sigma < 9.8$ the effective mass is smooth in the temperature, whereas for $g_\sigma > 9.8$ a phase transition of first order takes place.

To complete the characterization of the thermodynamics of this system, we examine the thermodynamic potential density, which will be normalized with respect to reference state $U(m_{\rm eff} = 0)$:

$$\frac{1}{V}[U(m_{\rm eff}) - U(m_{\rm eff} = 0)] \to \frac{U(m_{\rm eff})}{V}. \qquad (30)$$

Thus, in Figs. 3 and 4 the normalized thermodynamic potential density $U(T, \mu_{\rm eff} = 0)/V$, obtained by using Eq. (20) in (30), is plotted as a function of effective mass for $g_\sigma = 26.00$ and $g_\sigma = 16.00$, respectively, and for $m_\sigma = 0.53$. The discontinuous phase transition is clearly seen as T increases; the absolute minimum of the potential is displaced to a smaller value of $m_{\rm eff}$ as T increases. As suggested in Fig. 2, this first-order phase transition occurs at smaller critical temperatures as the magnitude of interaction between the σ and the ψ fields increases. For larger values of temperature, the effective mass decreases smoothly.

B. System with compactified spatial dimensions ($d = 1,2,3$)

Now we analyze the behavior of the effective mass under changes of the relevant parameters for the system with compactified spatial dimensions. Here we concentrate on the situation of larger values of g_σ, in which a phase transition of first order takes place.

In Fig. 5 are plotted the values of $m_{\rm eff}$ that are solutions of the gap equation in Eq. (22) as a function of temperature in the case of one compactified spatial dimension [with the scalar density being given by Eq. (24) for $d = 1$]. We see that allowed values of effective mass are affected by the presence the of boundary; the range of temperature where the mixed phase occurs is spread out as the length of compactified coordinate decreases. This result suggests that the symmetric phase is favored as the size of the system decreases. This will be better described via the plots involving the thermodynamic potential density, which will be done as follows.

In Figs. 6–8 are plotted the normalized thermodynamic potential density defined in Eq. (30) for $d = 1$ as a function of effective mass, taking different values of temperature, but with each plot at a given value of the size of the compactified coordinate. These three plots manifest the following nature of the transition: At smaller temperatures the global minimum is at a greater value of $m_{\rm eff}$; the increasing of T makes the second local minimum at a smaller value of $m_{\rm eff}$ overcome the first one, becoming the absolute minimum; for higher temperatures, the absolute minimum goes slightly to zero.

Besides, from Figs. 6–8 it can be seen that decreasing of the size L inhibits the broken phase, in agreement with the analysis

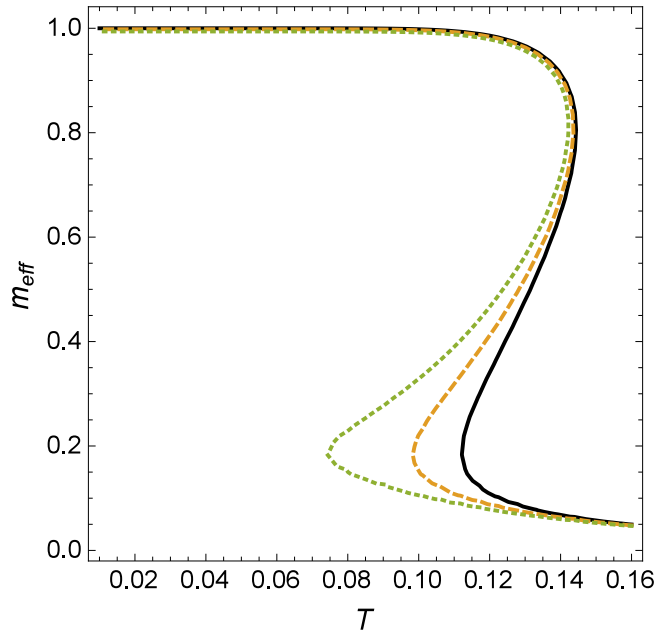

FIG. 5. Plot of values of $m_{\rm eff}$ that are solutions of the gap equation in Eq. (22) for $d = 1$ as a function of temperature, at chemical equilibrium. We fix $m_\sigma = 0.53$ and $g_\sigma = 26.00$. Solid, dashed, and dotted lines represent, respectively, $L = 15.00$, $L = 10.00$, and $L = 9.00$.

concerning Fig. 5. In other words, smaller values of L induce a first-order phase transition at lower critical temperatures.

Also, we plot in Fig. 9 the values of effective mass that are solutions of the gap equation in Eq. (22) as a function of inverse of length ($x = 1/L$), in the case of one compactified spatial dimension [with the scalar density being given by Eq. (24) for $d = 1$]. We notice that $m_{\rm eff}$ remains without change at greater values of L, where the fluctuations due to size effects are not relevant. However, we remark that the decreasing of the size of the system induces a sudden drop in $m_{\rm eff}$. Namely, there is a critical length L_c of the compactified dimension at which a discontinuous phase transition occurs. Besides, lower values of L_c are induced for smaller temperatures.

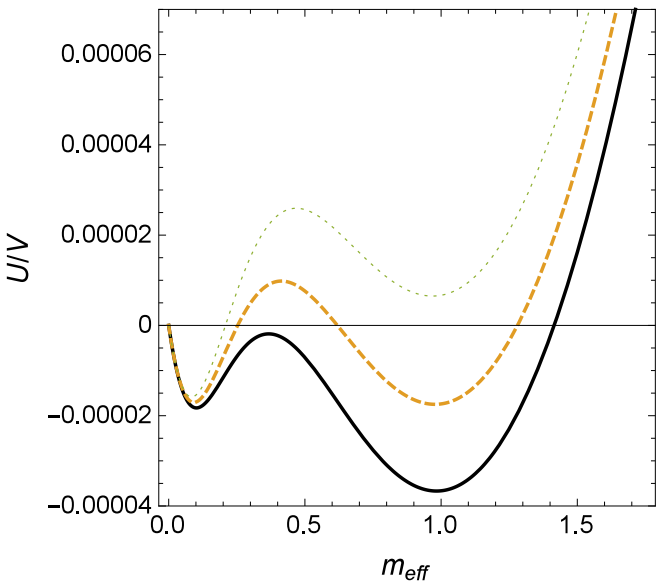

FIG. 6. Plot of normalized thermodynamic potential density in Eq. (30) for $d = 1$ as a function of effective mass and at chemical equilibrium. We fix $m_\sigma = 0.53$, $g_\sigma = 26.00$, and $L = 15.00$. Solid, dashed, and dotted lines represent the cases for $T = 0.1220$, $T = 0.1254$, and $T = 0.1293$, respectively.

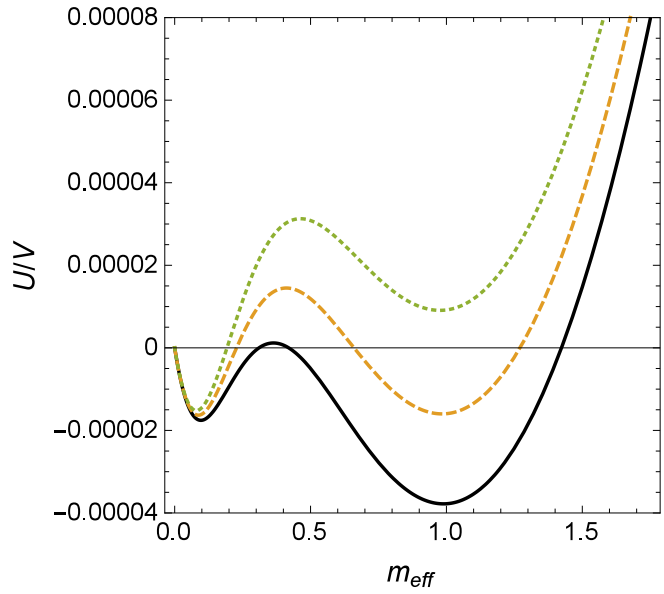

FIG. 7. Same as in Fig. 6, but with $L = 10.00$. Solid, dashed, and dotted lines represent the cases for $T = 0.1150$, $T = 0.1200$, and $T = 0.1250$, respectively.

We continue our discussion with Fig. 10, in which is plotted the normalized thermodynamic potential density defined in Eq. (30) for $d = 1$ as a function of effective mass, taking different values of L and at a fixed temperature. It can be

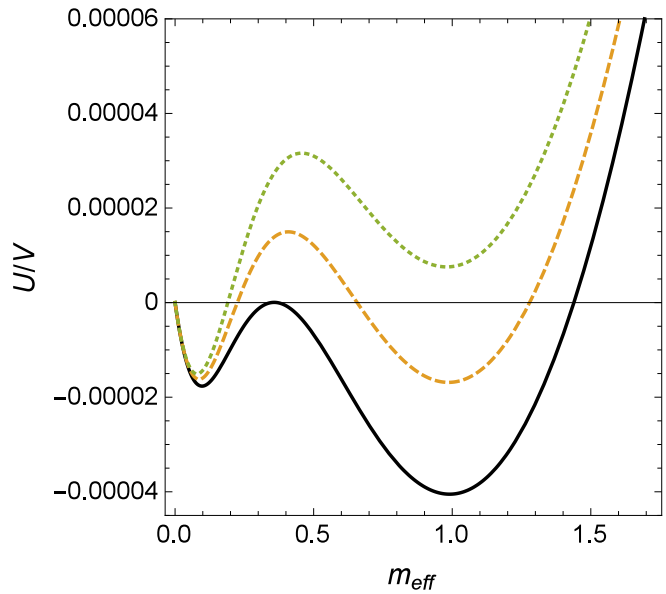

FIG. 8. Same as in Fig. 6, but with $L = 9.00$. Solid, dashed, and dotted lines represent the cases for $T = 0.1050$, $T = 0.1127$, and $T = 0.1190$, respectively.

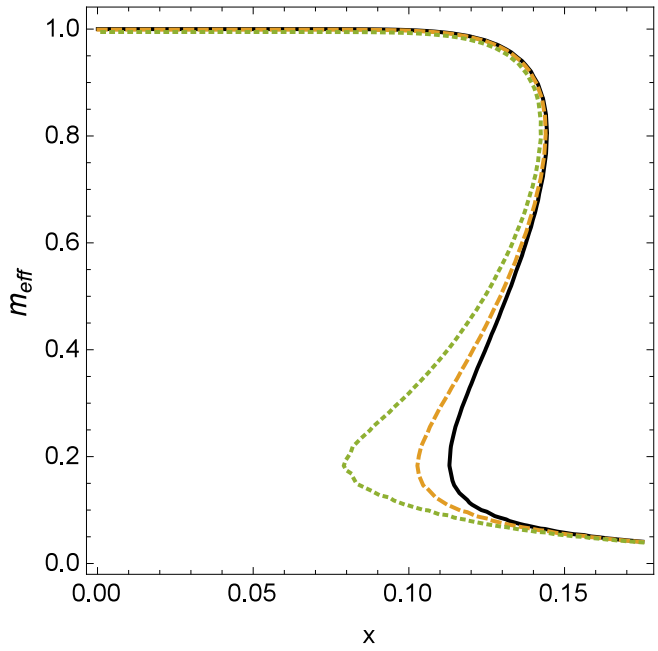

FIG. 9. Plot of values of m_{eff} that are solutions of the gap equation in Eq. (22) for $d = 1$ as a function of inverse of length ($x = 1/L$) at chemical equilibrium. We fix $m_\sigma = 0.53$ and $g_\sigma = 26.00$. Solid, dashed, and dotted lines represent, respectively, $T = 0.050$, $T = 0.095$, and $T = 0.110$.

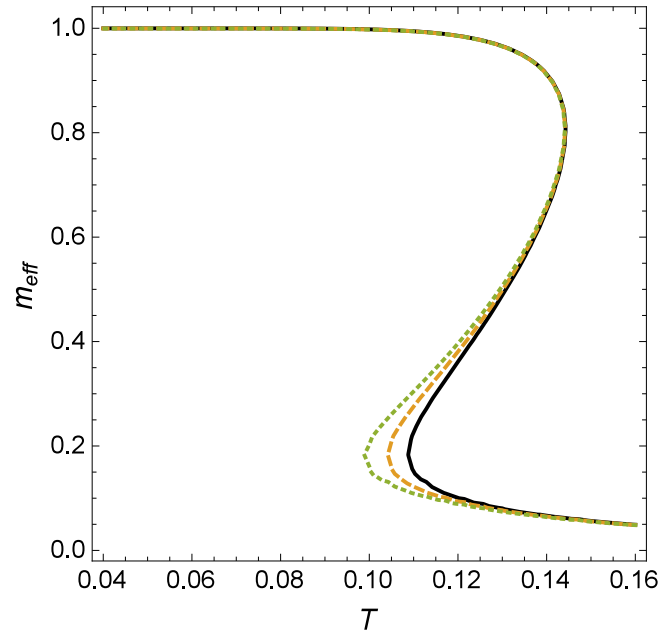

FIG. 11. Plot of values of m_{eff} that are solutions of the gap equation in Eq. (22) as a function of temperature, at chemical equilibrium. We fix $m_\sigma = 0.53$, $g_\sigma = 26.00$, and $L = 12.00$. Solid, dashed, and dotted lines represent, respectively, the case of $d = 1$, $d = 2$, and $d = 3$ compactified spatial dimensions.

seen that the global minimum of the system is discontinuously driven from the regime of greater values of m_{eff} to smaller ones, and it goes slightly to zero as L diminishes.

We conclude this investigation with the dependence of the phase structure on the number of compactified spatial dimensions. Then, in Fig. 11 are plotted the values of effective mass that are solutions of the gap equation as a function of temperature, for the three situations of compactified spatial dimensions under study with same length L, which is kept fixed. Precisely, in this plot is shown the solutions of Eq. (22), with

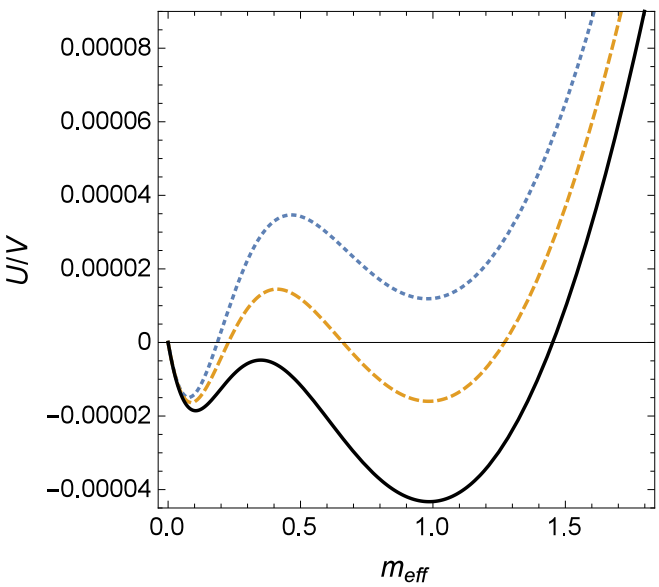

FIG. 10. Plot of normalized thermodynamic potential density in Eq. (30) for $d = 1$ as a function of effective mass and at chemical equilibrium. We fix $m_\sigma = 0.53$, $g_\sigma = 26.00$, and $T = 0.120$. Solid, dashed, and dotted lines represent the cases for $L = 13.00$, $L = 10.00$, and $L = 9.00$, respectively.

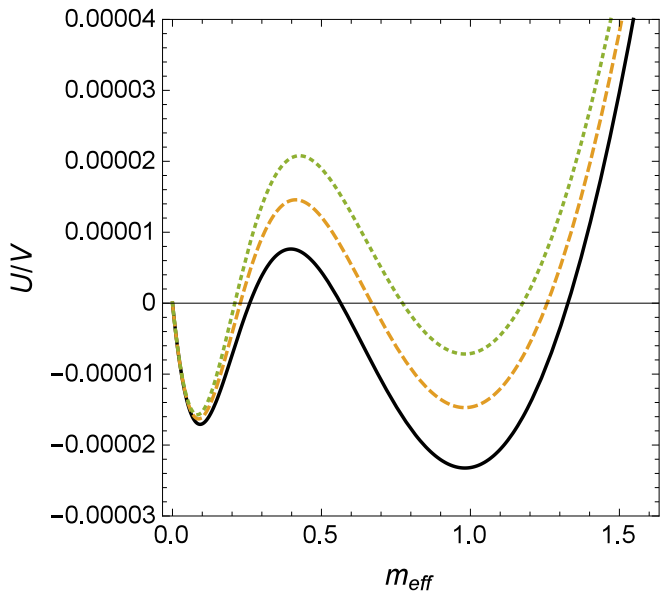

FIG. 12. Plot of normalized thermodynamic potential density in Eq. (30) as a function of effective mass and at chemical equilibrium. We fix $m_\sigma = 0.53$, $g_\sigma = 26.00$, $L = 12.00$, and $T = 0.123$. Dotted, dashed, and solid lines represent the cases for $d = 3$, $d = 2$, and $d = 1$, respectively.

the scalar density being given by Eq. (27) for $d = 1$ and analog expressions for $d = 2,3$, setting $L_i = L$ in each case. We remark that the range of temperature in which the mixed phase occurs is spread out as the number of compactified dimensions grows, with the symmetric phase being favored for bigger values of d. That is, one of the consequences of increasing of the number of compactified spatial dimensions is to cause the decreasing of the temperature at which transition occurs.

Once more, the analysis is completed with the normalized thermodynamic potential density defined in Eq. (30) for three situations of compactified spatial dimensions with the same length L, as a function of effective mass, at fixed values of temperature and length L. This plot is presented in Fig. 12. It can be seen that the system is driven from the broken to the disordered phase as the number of compactified spatial coordinates d increases. In other words, our findings suggest that the presence of more boundaries disfavors the maintenance of long-range correlations, making the suppression of the ordered phase.

IV. CONCLUDING REMARKS

In this work we have investigated the finite-size effects on the phase structure of the Walecka model within the framework of generalized ζ function, focusing on the influence of temperature, as well as the number and length $L_i = L$ of compactified spatial dimensions. As pointed out in previous papers, the nature of the phase transition strongly depends on the strength of the coupling constant g_σ. Here we have concentrated on the situation of larger values of g_σ, in which a phase transition of first order takes place. The main results obtained are summarized as follows.

We have seen that allowed values of effective mass are affected by the presence of boundaries; the range of temperature where the mixed phase occurs is spread as the length of compactified coordinates decreases. This result suggests that the symmetric phase is favored as the size of the system diminishes. In this sense, the decreasing of the size of the system induces a sudden drop in m_{eff}. It is suggested that a critical length L_c of the compactified dimensions at which a discontinuous phase transition occurs, and lower values of L_c are induced for smaller temperatures.

Besides, it has been remarked that the thermodynamic behavior of the system depends on the number of compactified spatial dimensions d. The symmetric phase is favored for bigger values of d with decreasing of the critical temperature. The presence of more boundaries tends to inhibit the broken phase. In other words, our findings suggest that the presence of more boundaries disfavors the maintenance of long-range correlations, inhibiting the broken phase.

Finally, we remark that the findings outlined above may give us insights about relativistic systems that can be interpreted as a fermion gas in a hot medium confined in a reservoir. Further studies will be done to apply the present approach to a specific physical system, such as nuclear matter. Moreover, the present analysis can be considered a starting point for further work in which the quantum corrections might be considered.

ACKNOWLEDGMENTS

The authors would like to thank the Brazilian funding agencies CNPq and CAPES for financial support.

[1] M. Le Bellac, *Thermal Field Theory* (Cambridge University Press, Cambridge, UK, 1996).
[2] J. I. Kapusta and C. Gale, *Finite Temperature Field Theory: Principles and Applications* (Cambridge University Press, Cambridge, UK, 2006).
[3] J. D. Walecka, Ann. Phys. **83**, 491 (1974).
[4] J. Theis, G. Graebner, G. Buchwald, J. Maruhn, W. Greiner, H. Stocker, and J. Polonyi, Phys. Rev. D **28**, 2286 (1983).
[5] A. Akmal, V. R. Pandharipande, and D. G. Ravenhall, Phys. Rev. C **58**, 1804 (1998).
[6] K. Saito, K. Tsushima, D. H. Lu, and A. W. Thomas, Phys. Rev. C **59**, 1203 (1999).
[7] S. A. Bass *et al.*, Prog. Part. Nucl. Phys. **41**, 255 (1998).
[8] M. Bender, P. H. Heenen, and P. G. Reinhard, Rev. Mod. Phys. **75**, 121 (2003).
[9] F. Weber, Prog. Part. Nucl. Phys. **54**, 193 (2005).
[10] B. A. Li, L. W. Chen, and C. M. Ko, Phys. Rep. **464**, 113 (2008).
[11] A. Delfino, M. Jansen, and V. S. Timoteo, Phys. Rev. C **78**, 034909 (2008).
[12] A. Lavagno, Phys. Rev. C **81**, 044909 (2010).
[13] R. S. Hayano and T. Hatsuda, Rev. Mod. Phys. **82**, 2949 (2010).
[14] X. Roca-Maza, X. Viñas, M. Centelles, P. Ring, and P. Schuck, Phys. Rev. C **84**, 054309 (2011); **93**, 069905(E) (2016).
[15] K. Fukushima and C. Sasaki, Prog. Part. Nucl. Phys. **72**, 99 (2013).
[16] R. H. Casali, L. B. Castro, and D. P. Menezes, Phys. Rev. C **89**, 015805 (2014).
[17] M. Dutra, O. Lourenco, S. S. Avancini, B. V. Carlson, A. Delfino, D. P. Menezes, C. Providencia, S. Typel, and J. R. Stone, Phys. Rev. C **90**, 055203 (2014).
[18] C. Mondal, B. K. Agrawal, and J. N. De, Phys. Rev. C **92**, 024302 (2015).
[19] K. A. Maslov, E. E. Kolomeitsev, and D. N. Voskresensky, Nucl. Phys. A **950**, 64 (2016).
[20] Z. W. Zhang and L. W. Chen, Phys. Rev. C **95**, 064330 (2017).
[21] M. Oertel, M. Hempel, T. Klahn, and S. Typel, Rev. Mod. Phys. **89**, 015007 (2017).
[22] L. M. Abreu, M. Gomes, and A. J. da Silva, Phys. Lett. B **642**, 551 (2006).
[23] D. Ebert, K. G. Klimenko, A. V. Tyukov, and V. Ch. Zhukovsky, Phys. Rev. D **78**, 045008 (2008).
[24] D. Ebert and K. G. Klimenko, Phys. Rev. D **82**, 025018 (2010).
[25] M. Hayashi and T. Inagaki, Int. J. Mod. Phys. A **25**, 3353 (2010).
[26] L. M. Abreu, A. P. C. Malbouisson, J. M. C. Malbouisson, and A. E. Santana, Nucl. Phys. B **819**, 127 (2011).
[27] J. Braun, B. Klein, and P. Piasecki, Eur. Phys. J. C **71**, 1576 (2011).

[28] L. F. Palhares, E. S. Fraga, and T. Kodama, J. Phys. G: Nucl. Part. Phys. **38**, 085101 (2011).
[29] L. M. Abreu, A. P. C. Malbouisson, and J. M. C. Malbouisson, Phys. Rev. D **84**, 065036 (2011).
[30] J. Braun, B. Klein, and B.-J. Schaefer, Phys. Lett. B **713**, 216 (2012).
[31] A. Flachi, Phys. Rev. D **86**, 104047 (2012).
[32] D. Ebert, T. G. Khunjua, K. G. Klimenko, and V. C. Zhukovsky, Int. J. Mod. Phys. A **27**, 1250162 (2012).
[33] A. Bhattacharyya, P. Deb, S. K. Ghosh, R. Ray, and S. Sur, Phys. Rev. D **87**, 054009 (2013).
[34] B. A. Berg and H. Wu, Phys. Rev. D **88**, 074507 (2013).
[35] L. M. Abreu, C. A. Linhares, A. P. C. Malbouisson, and J. M. C. Malbouisson, Phys. Rev. D **88**, 107701 (2013).
[36] L. M. Abreu, A. P. C. Malbouisson, J. M. C. Malbouisson, E. S. Nery, and R. Rodrigues da Silva, Nucl. Phys. B **881**, 327 (2014).
[37] D. Ebert, T. G. Khunjua, K. G. Klimenko, and V. C. Zhukovsky, Phys. Rev. D **91**, 105024 (2015).
[38] F. C. Khanna, A. P. C. Malbouisson, J. M. C. Malbouisson, and A. E. Santana, Phys. Rep. **539**, 135 (2014).
[39] A. Bhattacharyya, R. Ray, S. Samanta, and S. Sur, Phys. Rev. C **91**, 041901 (2015).
[40] A. Bhattacharyya, R. Ray, and S. Sur, Phys. Rev. D **91**, 051501 (2015).
[41] L. M. Abreu, E. S. Nery, and A. P. C. Malbouisson, Phys. Rev. D **91**, 087701 (2015).
[42] L. M. Abreu and E. S. Nery, Int. J. Mod. Phys. A **31**, 1650128 (2016).
[43] L. M. Abreu, A. P. C. Malbouisson, and E. S. Nery, Mod. Phys. Lett. A **31**, 1650121 (2016).
[44] A. Bhattacharyya, S. K. Ghosh, R. Ray, K. Saha, and S. Upadhaya, Europhys. Lett. **116**, 52001 (2016).
[45] N. Magdy, M. Csanád, and R. A. Lacey, J. Phys. G: Nucl. Part. Phys. **44**, 025101 (2017).
[46] K. Redlich and K. Zalewski, arXiv:1611.03746 [nucl-th].
[47] H. J. Xu, Phys. Lett. B **765**, 188 (2017).
[48] S. Samanta, S. Ghosh, and B. Mohanty, arXiv:1706.07709 [hep-ph].
[49] T. Matsubara, Prog. Theor. Phys. **14**, 351 (1955).
[50] F. C. Khanna, A. P. C. Malbouisson, J. M. C. Malbouisson, and A. E. Santana, *Quantum Field Theory on Toroidal Topology: Algebraic Structure and Applications* (World Scientific, Singapore, 2009).
[51] E. Elizalde, *Ten Physical Applications of Spectral ζ Function*, Lecture Notes in Physics (Springer-Verlag, Berlin, 1995).
[52] S. A. Chin, Phys. Lett. B **62**, 263 (1976).
[53] R. A. Freedman, Phys. Lett. B **71**, 369 (1977).
[54] T. Matsui and Brian D. Serot, Ann. Phys. (NY) **144**, 107 (1982).